

Article

# Human Limb Motion Detection with Novel Flexible Capacitive Angle Sensor Based on Conductive Textile

Jian-Feng Wu <sup>1,2,\*</sup> , Chao Qiu <sup>1</sup>, Yu Wang <sup>1</sup>, Rui Zhao <sup>1,3</sup>, Zhi-Peng Cai <sup>1</sup>, Xin-Gang Zhao <sup>2</sup>, Shang-Shang He <sup>1</sup>, Feng Wang <sup>1</sup>, Qi Wang <sup>1</sup> and Jian-Qing Li <sup>1</sup>

<sup>1</sup> State Key Laboratory of Bioelectronics, Jiangsu Key Lab of Remote Measurement and Control, School of Instrument Science and Engineering, Southeast University, Nanjing 210096, China; 220173188@seu.edu.cn (C.Q.); 220152746@seu.edu.cn (Y.W.); rzhao001@e.ntu.edu.sg (R.Z.); 230169212@seu.edu.cn (Z.-P.C.); 220152718@seu.edu.cn (S.-S.H.); 220162828@seu.edu.cn (F.W.); 220162762@seu.edu.cn (Q.W.); ljq@seu.edu.cn (J.-Q.L.)

<sup>2</sup> State Key Laboratory of Robotics, Shenyang Institute of Automation, Chinese Academy of Sciences, Shenyang 110016, China; zhaoxingang@sia.cn

<sup>3</sup> Harveston Asset Management, Singapore 069542, Singapore

\* Correspondence: wjf@seu.edu.cn; Tel.: +86-153-6600-6069

Received: 2 August 2018; Accepted: 9 September 2018; Published: 11 September 2018



**Abstract:** In recent years, many sensors made of hard materials have been designed to detect human body movements in physical exercises. However, hard materials usually cause extra dyskinesia for body movements. To detect human limb motion with less dyskinesia in physical exercise, a novel flexible capacitive angle sensor (NFCAS) based on a conductive textile was designed in this paper. The NFCAS has two non-parallel plates, namely, an exciting plate and a sensing plate, which can be fixed onto the inner forearm and the inner upper arm. Thus, the angle between the two plates of the NFCAS can be used to represent the angle of medial elbow, and its variation can lead to changes in the sensor's capacitance at the same time. A push-ups experiment and pull-ups experiment were conducted to evaluate the designed NFCAS's performance. Experimental results showed that the NFCAS could detect the main processes of push-ups and pull-ups. Besides high measurement precision, the NFCAS is also soft, thin, lightweight, and easily made. Therefore, it can be widely applied for detecting human limb motion with less dyskinesia in physical exercises.

**Keywords:** motion detection; flexible capacitive angle sensor; conductive textile

## 1. Introduction

Non-contact sensors and contact sensors have been designed to detect human body motion. A comparison of different human body motion detection sensors is shown in Table 1. Typical non-contact sensors, e.g., Kinect sensors, are widely used to detect human postures and gestures in human-computer interactions and somatosensory gaming. Yunda Liu et al. [1] proposed a dynamic gesture-recognition method based on Kinect sensors. G. Kurillo et al. [2] evaluated the reachable workspace of the upper limb using Kinect sensors without any extra dyskinesia. However, Kinect sensors require the subject to stay within a relatively small space, which limits its applications on human body detection in outdoor physical exercise that normally needs larger space [3]. Contact sensors, which consist of two types—non-flexible sensors and flexible sensors—are widely used in human health monitoring in outdoor environments. Non-flexible sensors, such as inertial measurement units (IMUs) and magneto and inertial measurement units (M-IMUs), are usually made of hard materials, which could cause extra dyskinesia to users. IMU [4–6] and M-IMU sensors [7] were used to detect human body motion in outdoor physical exercises. T. Seel et al. [4] proposed a method based on IMU

sensors to calculate joint-motion angles in gait analyses. In most scenarios, IMU sensors with small size and light weight required more integral calculations, that might lead to extra errors. M. H. Imtiaz et al. designed a multisensory wearable system with IMU to track hand-to-mouth gestures. L. Ricci et al. [7] analyzed children's motion in daily life by capturing the thorax and upper limb motion with M-IMU sensors. M-IMU sensors had higher precision than IMU, but its data acquisition process required complex post-processing. At the same time, M-IMU might fail because magnetometers are sensitive to external spatial electro-magnetic noises. Furthermore, non-flexible sensors could cause extra dyskinesia. Therefore, soft sensors are required, especially in continuous detection of human body movements, to tackle the above issues [8]. Flexible strain sensors, which are made of soft materials and cause less extra dyskinesia to users, can be categorized into strain-resistive sensors and strain-capacitive sensors. Based on knitted piezoresistive fabrics, Bianchi M. et al. [3] developed a multi-modal sensing glove to detect human manual-interaction. T. W. Shyr et al. [9] designed a wearable gesture-sensing device based on a textile strain resistive sensor, whose resistance is related to its flexion angle in a linear manner. However, steady fabric, which has been used to fix the textile strain sensor, always causes discomfort and small strain dyskinesia to the users. Repeated and intensive motion might change the position of the textile strain resistive sensors, which could decrease the sensors' detection precision. H. Nakamoto et al. [10] designed a flexible and stretchable strain capacitive sensor with a sandwiched structure. Flexible sensors are thin, light weight, and elastic. However, these sensors are only effective via touching users' skin, so users may feel uncomfortable, and the whole installation and removal processes are going to become more complicated and annoying.

**Table 1.** Comparison of different human body motion detecting sensors.

Reference	Type	Sensor	Advantages	Disadvantages
[1,2]	Non-contact	Kinect sensor	Without any dyskinesia	Limitation of applying situation
[4–6]	Contact and non-flexible	IMU sensor	Small size, lightweight	Extra dyskinesia, post-processing
[7]	Contact and non-flexible	M-IMU sensor	High precision	Extra dyskinesia, more complex, post-processing, susceptible to interference
[3,5,9,10]	Contact and flexible	Strain resistive sensor	Flexible, light weight	Strain dyskinesia, discomfort
[8]	Contact and flexible	Strain capacitive sensor	Elastic, thin, light weight	Strain dyskinesia, installation perplex, discomfort, removal processes
Proposed	Contact and flexible	NFCAS	Flexible, easy-made, low extra dyskinesia	Limitation range of detection angle

To achieve the good properties, i.e., easily made and working with low extra dyskinesia, a novel flexible capacitive angle sensor (NFCAS) for human motion detection in physical exercises has been designed and fabricated in this paper. The NFCAS was evaluated in several push-ups and pull-ups experiments. This paper is organized as follows: in Section 1, existing human motion sensors were reviewed and analyzed. Then, our proposed NFCAS will be introduced, covering its principal and fabrication in Section 2. Experimental studies will be presented in Section 3. Finally, a discussion and conclusion will be given in Section 4.

## 2. Detection Principle and Fabrication of the NFCAS

### 2.1. Detection Principle of the NFCAS

Capacitive sensors work based on changes of capacitance. The adjustment of various parameters, including dielectric permittivity, sensing area, and the distance between the two parallel electrode plates, changes the capacitances of the parallel-plate capacitive sensors, which can be used to measure various parameters, such as micro-displacement [11], pressure [12], flow [13], water level [14], and respiration [15]. In [16], some non-parallel-plate capacitive sensors based on the angle change

were reported. To detect the angle change of human limbs, a flexible capacitive sensor based on the non-parallel-plate capacitor has been designed in this paper. As shown in Figure 1a, the NFCAS has an exciting electrode plate (EEP) and a sensing electrode plate (SEP) to detect the angle of human limb. The EEP and the SEP of the NFCAS were fixed to the inner forearm and the inner upper arm. Thus, the angle between two non-parallel plates of the NFCAS could be used to represent the angle of medial elbow, and its variation could result in the change of the NFCAS's capacitance. A prototype detection system of the NFCAS is shown in Figure 1a.

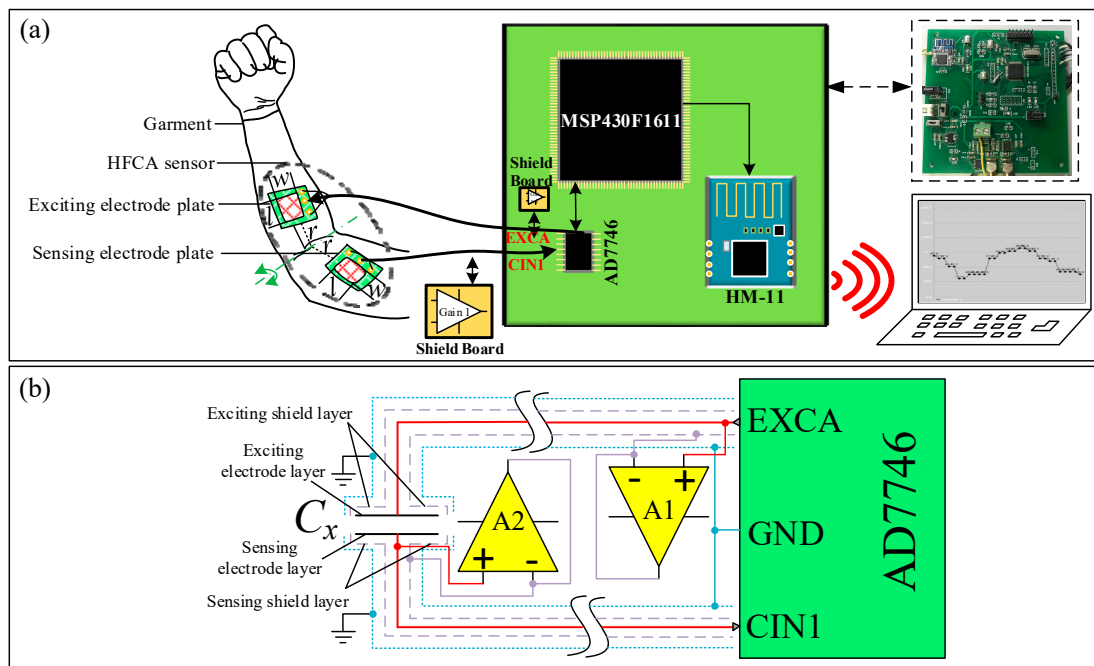


**Figure 1.** The NFCAS (a) Prototype detection system; (b) Detection circuit with drive cable technology.

A micro-capacitance detection chip (AD7746, Analog Devices, Inc., Norwood, MA, USA) [17] was used to measure the NFCAS's capacitance. In addition, a MSP430F1611 (TEXAS INSTRUMENTS, Dallas, TX, USA) and a Bluetooth 4.0 module (HM-11, HI-SINCERITY MICROELECTRONICS CORP., Taipei, China) were used as a controller and a remote communication port, respectively. A precision rail-to-rail operational amplifier (OP184, Analog Devices, Inc.) was used for putting the shield at the potential of the electrode. Four rechargeable batteries, each of 1.2 V, were used in series as the power input, with a total voltage of 4.8 V required for the prototype detection system. An AMS1117-3.3 chip (Advanced Monolithic Systems Inc., Livermore, CA, USA) was used to regulate the power voltage to 3.3 V. As shown in Figure 1b, the EXCA pin and the CIN1 pin were connected to the exciting electrode layer of the EEP and the sensing electrode layer of the SEP respectively. The AD7746 generated the excitation signal of a square wave fixed at 32 KHz. The measurement range was from 0 pF to 8.192 pF by programming compensation for the AD7746 in the single-end input mode. The AD7746 transmitted the primary data to the MSP430F1611 through its IIC Bus. After data conversion, the capacitance value was transmitted from the MSP430F1611 to a remote computer through the HM-11.

In Figure 1a, the NFCAS can be generally described as two non-parallel electrode plates. Under the assumption that fringe effect at the edges of the plates can be ignored if these two plates are of infinite width, the capacitance ( $C_x$ ) between the plates with the angle of  $\theta$  can be formulated by the Equation (1) [18]:

$$C_x = \frac{180\epsilon w}{\pi\theta} \ln\left(1 + \frac{l}{r}\right), \theta \in (0^\circ, 180^\circ] \quad (1)$$

where,  $\epsilon$  is air dielectric permittivity;  $r$  is the near radius of rotation of the NFCAS;  $l$  and  $w$  denote length and width of one conducting plate in the NFCAS, respectively.

However, in reality, the fringe effect of the electrode plates usually causes small interferences to  $C_x$ . However, it is difficult or even impossible to derive the exact formulation for  $C_x$ . Thus, in the general case,  $C_x$  can be approximately evaluated by Equation (1).

The detection circuit with drive cable technology for the NFCAS is shown in Figure 1b. Drive cable technology [19] was good for reducing the negative effect of parasitic capacitance caused by long test cables and fringe effect. Thus, it was adopted in the NFCAS, and special structures of the NFCAS and its test cables were designed. In Figure 1b, two operational amplifiers with a gain of 1 were used to achieve equipotential between the shielding layer and the signal layer for the EEP and the SEP respectively. Based on the NFCAS's structure, the structure of each cable was designed to contain three layers, namely, a signal layer, shielding layer, and ground layer. Therefore, the capacitor between the ground and signal layers becomes the operational amplifier's load. Consequently, two plates could be shielded from electric noise near the NFCAS to reduce the potential capacitive leakage and eliminate negative influences. As a result, the specific structures of the NFCAS and its corresponding test cables in the design can contribute a lot to the proper operation of our proposed NFCAS.

## 2.2. Fabrication of the NFCAS

Flexible materials, including flexible conductive textile and flexible laminating films, are very important to make the users' experience more comfortable. Flat conductive textiles exhibiting good electric conduction [20] have been widely used in recent years. The NFCAS's design methodology is shown in Figure 2a. The NFCAS consisted of two plates, i.e., the EEP and the SEP, that shared the same mechanical structure. The EEP was composed of three layers, i.e., the exciting electrode layer (EEL), the exciting shield layer (ESL), and the ground layer (GL), while the SEP was composed of three layers: the sensing electrode layer (SEL), the sensing shield layer (SSL), and the GL. All layers were made of conductive textile (SXG-1, Qingdao Hengtong X-silver Speciality Textile Co., Ltd., Qingdao, China). The SEP, as an example, is used to introduce the NFCAS's structure. The conductive textile has good electrical conductivity, stretchability, and flexibility after curing. For a sample cloth made of the conductive textile with its length of 127 mm and its width of 10 mm, its resistance was  $1.338 \Omega$  in our pre experiment with an Agilent 34401A multimeter. To avoid short circuits, two insulation layers were placed between any two of these three layers. Two insulation layers were also laid on the top and bottom of the NFCAS to protect the SEL and the GL. The insulation layers were made of laminating film (6.5C, Shanghai Wende culture and sports articles Co., Ltd., Shanghai, China). Polyethylene with the dielectric permittivity about 2.25 was the main component of the laminating film, with a thickness of 0.065 mm. Standard snap fasteners were used to connect the plates of the NFCAS to signal cables. As shown in Figure 2a, the NFCAS was fixed on the garment's surface to detect human limb motion. The EEP and the SEP were fixed at the inner forearm and the inner upper arm respectively. The two plates formed a non-parallel-plate capacitor. When the elbow was bent or stretched, both the angle between the EEP and the SEP and the NFCAS's capacitance changed.

Figure 2b shows the NFCAS's circuit schematic. With drive cable technology, each test cable of the NFCAS was composed of three layers: signal layer, shielding layer, and ground layer. The EEL of the EEP was connected to the EXCA pin of the AD7746 through its signal layer, the ESL of the EEP was connected to its shielding layer, and the GL was connected to the ground pin of the AD7746. Similarly, the SEL of the SEP was connected to the CIN1 pin of the AD7746, the SSL of the SEP was connected to its shielding layer, and the GL was connected to the ground pin of the AD7746. The operational amplifiers with closed loop gains of 1 were used to achieve equipotential between the ESL and the EEL, and equipotential between the SEL and the SSL. Thus, the capacitors between the ground layer and the signal layer became the loads of the operational amplifiers. Hence, capacitive leakage was eliminated, and the parasitic capacitance effect was overcome.

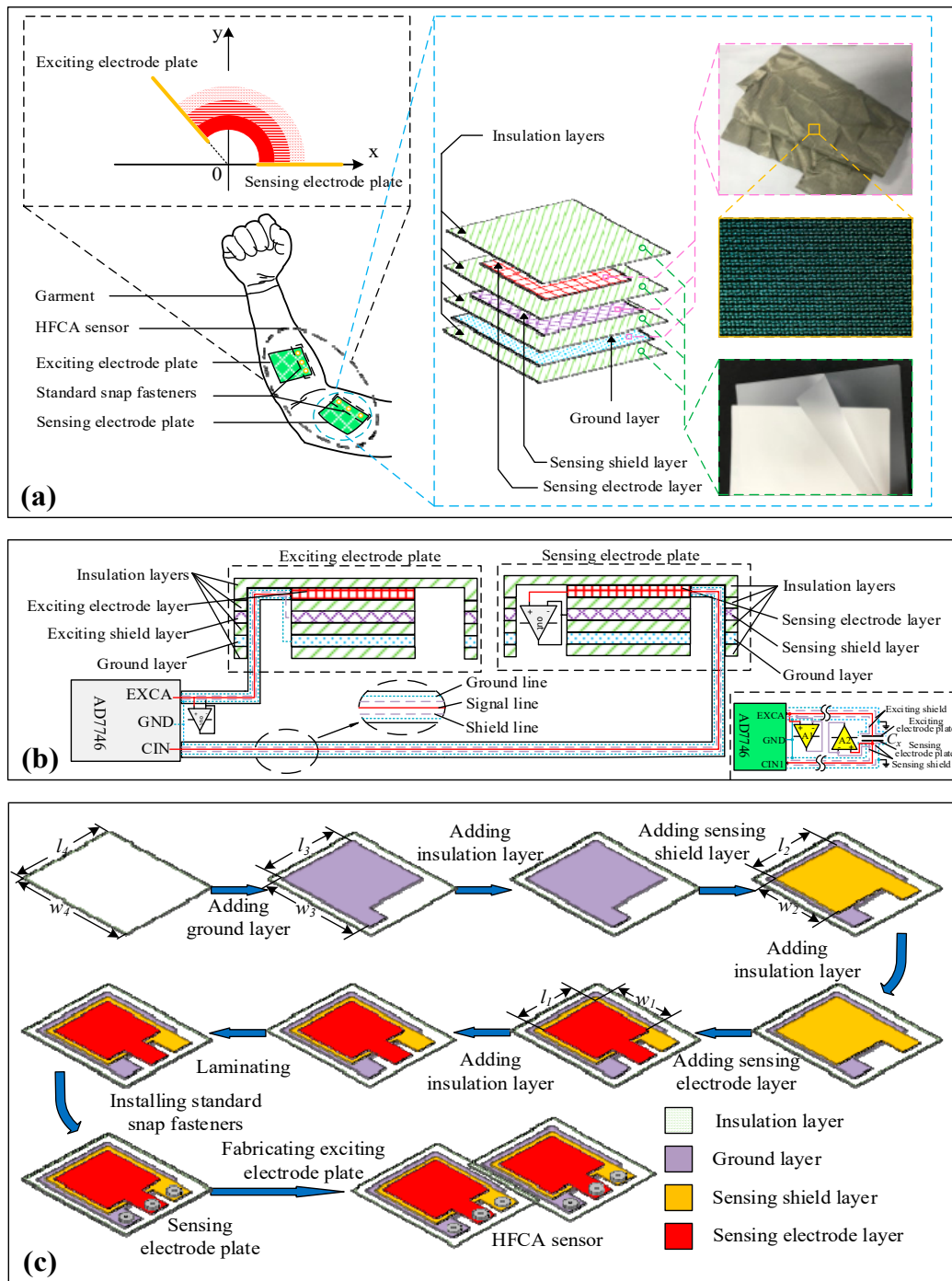


**Figure 2.** Fabrication of the NFCAS. (a) Schematic illustration of the NFCAS. Inserts: diagrams of the NFCAS’s model and structure, and images of the main materials of the NFCAS; (b) Circuit connection schematic of the NFCAS; (c) Fabrication process schematic for the NFCAS.

Figure 2c shows schematic of the fabrication process for the NFCAS. The SEP, as an example, is used to introduce the NFCAS’s structure. All layers should be prepared before fabricating the NFCAS. Firstly, the main parts and extended parts of the SEL, the SSL, and the GL were cut out from the conductive textile with sizes of  $l_1 \times w_1$ ,  $l_2 \times w_2$  and  $l_3 \times w_3$ . To ensure the shielding effects, these dimensions followed the relationship:  $l_1 < l_2 < l_3$ , and  $w_1 < w_2 < w_3$ . Secondly, the SEL, the SSL, and the GL were flattened by the laminator at 60 °C. Finally, all insulation layers were cut out with laminating film with sizes  $l_4$  ( $l_3 < l_4$ )  $\times$   $w_4$  ( $w_3 < w_4$ ).

As shown in Figure 2c, an insulation layer was first laid at the bottom. Then the GL was placed over it. To avoid a possible short circuit between the GL and SSL, another insulation layer was laid on the surface of the GL before the placement of SSL. To protect the SEL, its top surface was covered by an insulation layer. After being laminated at 78 °C, three standard snap fasteners with a diameter of 9.0 mm were installed in the extending part of the SEL, the SSL, and the GL, respectively, which can facilitate the transmitting of the signals of the sensors.

These soft materials are able to reduce the level of extra dyskinesia caused by the NFCAS. After the final lamination, the plates of the NFCAS can be kept soft with a very small thickness of each plate, i.e., 0.40 mm. In the fabrication of the NFCAS, Laminator (330C, Shanghai Wende culture and sports articles Co., Ltd.) was used.

### 3. Experiments and Results

In the experiments, unless otherwise noted,  $w_1$ ,  $l_1$ , and  $r$ , were set as 4.0 cm, 4.0 cm, and 3.0 cm, respectively. Two plates of the NFCAS were fixed to the inner sides of the medial elbow, and they were connected to the test circuit with cables of 33.0 cm length.

#### 3.1. Basic Experiments

##### 3.1.1. Calibration Experiment and Simulation Experiments

A calibration platform was set up with a MPU6050 (InvenSense Inc., San Jose, CA, USA). In the platform, the sensing electrode plate and the exciting electrode plate of the NFCAS were fixed on a horizontal cardboard and a rotatable cardboard respectively; the MPU6050 used as the angular reference was also fixed onto the rotatable cardboard. In the calibration experiment, the horizontal cardboard was fixed, and the rotatable cardboard was rotated from 10° to 180°, with the interval of 10°. Also, the two dimensional finite element analysis (2D FEA) experiment of the NFCAS with ANSYS software and the simulation experiment of the Equation (1) with MATLAB software (R2014a, MathWorks Inc., Natick, MA, USA) were carried out. The experimental results are shown in Figure 3.

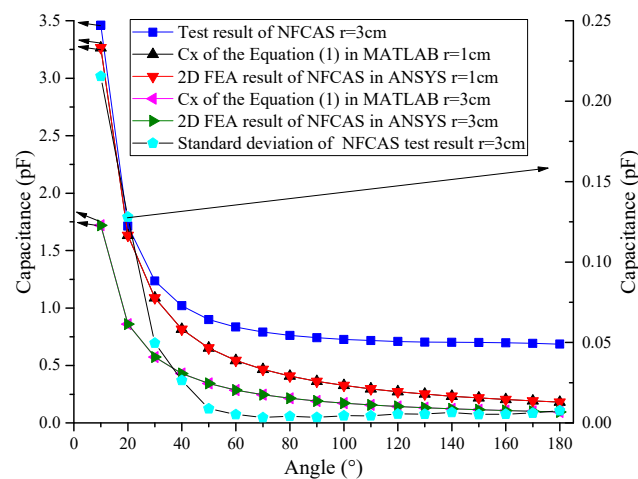


**Figure 3.** Results of the NFCAS in calibration experiments and analysis experiments.

From Figure 3, the simulation result of the Equation (1) in the MATLAB was very close to the 2D FEA experimental result in the ANSYS under the same conditions. The NFCAS's test result was larger than its computation capacitance of the Equation (1), and the larger the angle, the more significant the trend. The NFCAS's capacitance had an inverse ratio to the angle, i.e., a larger capacitance corresponds to a smaller angle, and vice versa. The NFCAS's capacitance's change is more sensitive to a small angle change under a smaller absolute angle. When the angle was larger than 80°, the change of the NFCAS's test result was insignificant. The standard deviation of the NFCAS's test result is inversely

related to the angle. As shown in the Figure 3, the standard deviation was large when the angle was small ( $\leq 40^\circ$ ), while it was small ( $<0.01$  pF) when the angle was larger than  $50^\circ$ .

### 3.1.2. Experiments of Forearm Rotation and Arm Muscle Deformation

Based on the angle-capacitance curve of the NFCAS shown in Figure 3, the angle of the medial elbow could be calculated with the measured capacitance. In physical exercises, forearm could rotate and arm muscle could deform, which affected the surface morphologies of the forearm and the upper arm. Thus, the NFCAS's results would be affected by forearm rotation and arm muscle deformation. In the experiments of forearm rotation and arm muscle deformation, two MPU6050s were used. One MPU6050 and the NFCAS's EEP were fixed on the inner forearm at the same time, the other MPU6050 and the NFCAS's SEP were fixed on the inner upper arm simultaneously. In these experiments, the angle of medial elbow was changed from  $30^\circ$  to  $150^\circ$ . At each angle, the subject's forearm had three action states: muscle relaxation (Opening palm in relaxation), muscle contraction (Clenching a fist), and rotation (Opening palm in relaxation and rotating the forearm about  $150^\circ$  against the clockwise). The experimental results are shown Figure 4.

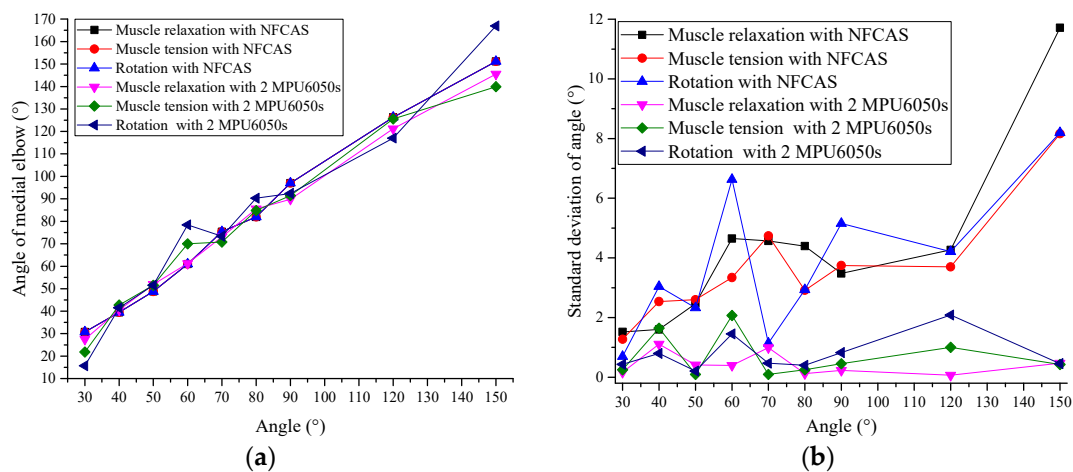


**Figure 4.** Experimental results of forearm rotation and muscle deformation. (a) Angle of medial elbow; (b) Standard deviation of angle.

From Figure 4, both the NFCAS and the MPU6050s could detect the change of the medial elbow's angle. Standard deviations of angle results with the NFCAS were larger than those with the MPU6050s ( $<2.1^\circ$ ). With an increase of the angle, the NFCAS's standard deviations increased. Both the NFCAS's results and the MPU6050s' results were affected by the forearm's state, including muscle relaxation, muscle contraction, and rotation, in which the forearm's rotation caused obvious irregular measurement errors in both the NFCAS and the MPU6050s.

### 3.2. Pull-Ups Experiment and Push-Ups Experiment

As shown in Figure 5, a garment with hook-and-loop fasteners was used to fix the NFCAS. Thus, the NFCAS can be easily worn or removed. The hook-and-loop fasteners were cut into patches of appropriate sizes. The loop side of the tape was sewn at the surface of garment base, while the hook side was glued to the bottom of the plate of the sensor. In Figure 6, the EEP and the SEP were fixed onto the inner forearm and the inner upper arm respectively. In addition, the NFCAS's effectiveness was verified by comparing the performances of a MPU6050 sensor fixed on the inner upper arm. Push-ups and pull-ups experiments were conducted to verify the performance of the NFCAS. In the experiments,  $\theta$  is the angle between the upper arm and the former arm detected by the NFCAS,  $\alpha$  is the angle between the upper arm and the horizontal surface detected by the MPU6050, and  $C_x$  is the NFCAS's capacitance.

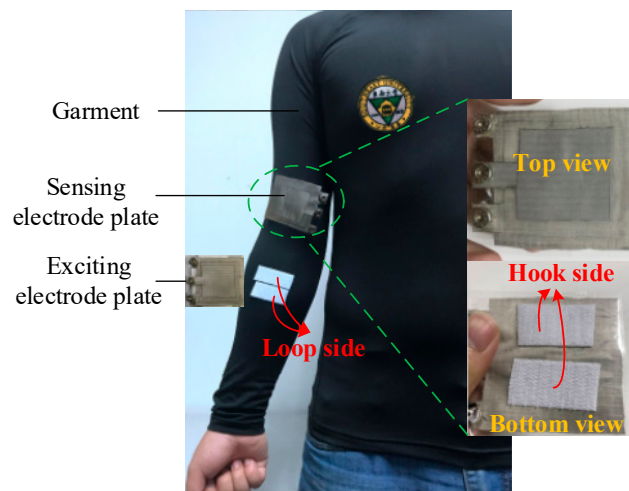


Figure 5. A garment with hook-and-loop fasteners used to fix the NFCAS.

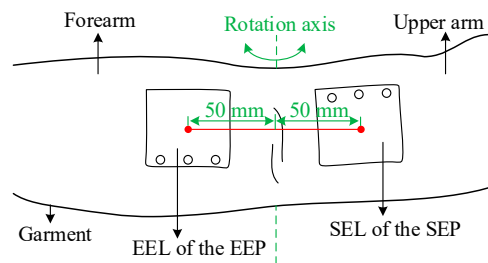


Figure 6. Schematic of installation position of the NFCAS.

### 3.2.1. Pull-Ups Experiment

In pull-ups experiment, a human arm was transformed into the stick model with upper arm and forearm as shown in Figure 7. The experimental results are shown Figure 8.

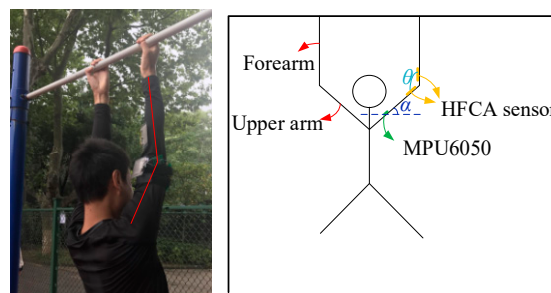
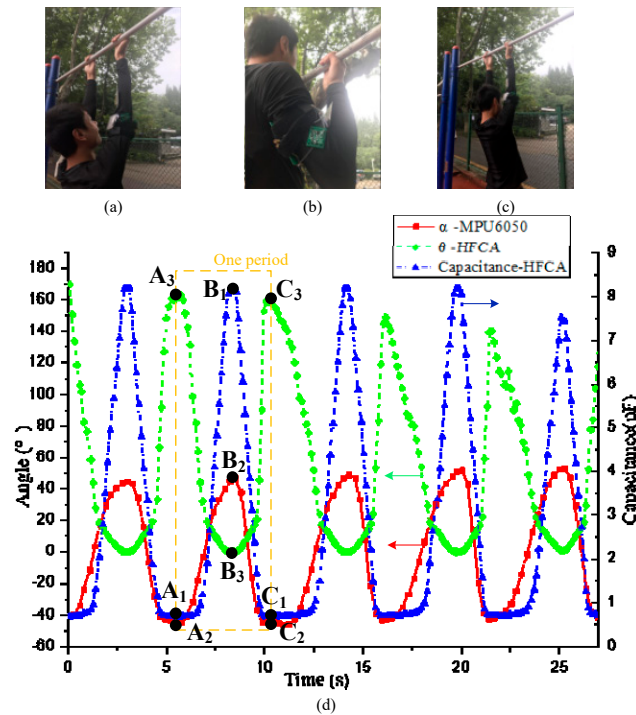


Figure 7. The detection model of pull-ups.

In Figure 8a–c, the process of pull-ups was divided into three parts: (1) preparation; (2) pulling process; and (3) hanging down. In Figure 8d, the square-data curve, the diamond-data curve, and the triangle-data curve represent  $\alpha$ ,  $\theta$ , and  $C_x$ , respectively. The complete pull-ups motion cycle represents the yellow dashed rectangle frame. The ranges of  $\alpha$ ,  $\theta$ , and  $C_x$  were in  $-50^\circ$  to  $50^\circ$ ,  $0^\circ$  to  $180^\circ$ , and 0.6 pF to 8.192 pF (full range), respectively. The participant was in preparation at point  $A_1$  in the triangle-data curve, at point  $A_2$  in the square-data curve, and at point  $A_3$  in the diamond-data curve. From point  $A_1$  to point  $B_1$  in the triangle-data curve, from point  $A_2$  to point  $B_2$  in the square-data curve, and from point  $A_3$  to point  $B_3$  in the diamond-data curve, the participant bent the elbow and pulled upward. In this process,  $\alpha$ ,  $\theta$ , and  $C_x$  were changed from the minimum ( $-50^\circ$ ) to the maximum ( $50^\circ$ ),  $170^\circ$  to about  $0^\circ$ , and the minimum (0.6 pF) to full range (8.192 pF), respectively. From point  $B_1$  to point  $C_1$  in the triangle-data curve, from point  $B_2$  to point  $C_2$  in the square-data curve, and from point  $B_3$  to

point  $C_3$  in the diamond-data curve, the participant dropped from the highest to the lowest position. The values in the triangle-data curve and square-data curve also dropped from the maximum to the minimum. At the same time,  $\theta$  changed from about  $0^\circ$  to  $170^\circ$ . From Figure 8d, the change of  $\theta$  corresponded to the change of  $\alpha$ , and the NFCAS's capacitance showed a small change when  $\theta$  was changed in  $80^\circ \sim 170^\circ$ .



**Figure 8.** Pull-ups experimental results. (a) Preparation; (b) Pulling status; (c) Hanging down; (d) Experimental results.

### 3.2.2. Push-Ups Experiment

In the push-ups experiment, as shown in Figure 9, a human body was transformed into the stick model, which consists of upper arm and forearm. The experimental results are shown Figure 10.

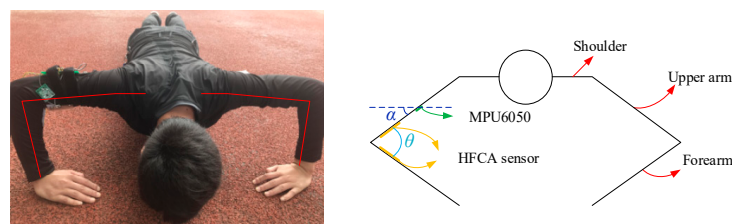


**Figure 9.** The detection model of push-ups.

In Figure 10a–c, the process of push-ups was divided into three parts: (1) preparation; (2) descending process; and (3) pushing process. In Figure 10d, the square-data curve indicated  $\alpha$ , the diamond-data curve indicated  $\theta$ , and the triangle-data curve indicated  $C_x$ . The yellow dashed rectangle frame represented a complete push-ups motion cycle. The ranges of  $\alpha$ ,  $\theta$ , and  $C_x$  were in  $10^\circ$  to  $80^\circ$ ,  $0^\circ$  to  $180^\circ$ , and  $0.6$  pF to  $8.192$  pF (full range), respectively. The participant was in preparation at point  $A_1$  in the triangle-data curve, at point  $A_2$  in the square-data curve, and at point  $A_3$  in the diamond-data curve. From point  $A_1$  to point  $B_1$  in the triangle-data curve, from point  $A_2$  to point  $B_2$  in the square-data curve, and from point  $A_3$  to point  $B_3$  in the diamond-data curve, the participant completed a descending movement. In this process,  $\alpha$  and  $\theta$  changed from the maximum to the

minimum, respectively. At the same time,  $C_x$  changed from the minimum to its maximum. With the arm stretching straight (from point  $B_1$  to point  $C_1$  in the triangle-data curve, from point  $B_2$  to point  $C_2$  in the square-data curve, and from point  $B_3$  to point  $C_3$  in the diamond-data curve),  $\alpha$  and  $\theta$  changed from the minimum to the maximum, respectively, and  $C_x$  changed from the maximum to the minimum. From Figure 10d, similar to the results in Figure 8d, the change of  $\theta$  corresponded to the change of  $\alpha$ , and the NFCAS's capacitance showed a small change when  $\theta$  was larger than  $80^\circ$ . The triangle-data curve of  $\theta$  fluctuated significantly when  $\theta$  was larger than  $80^\circ$ .

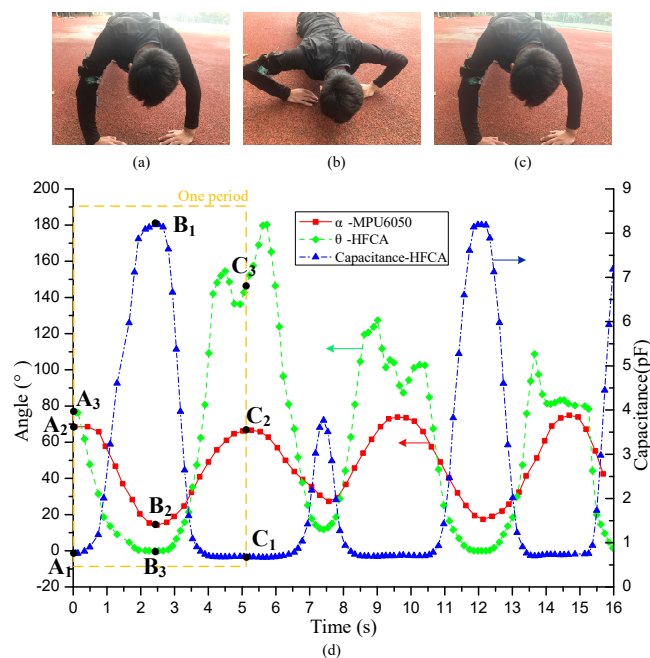


**Figure 10.** Push-ups experimental results. (a) The preparation; (b) The descending status; (c) The pushing status; (d) Experimental results.

#### 4. Discussion and Conclusions

A NFCAS consisting of an exciting electrode plate and a sensing electrode plate was designed in this paper. In order to eliminate the capacitance leakage and to overcome the interference of parasitic capacitance, specified structures of the NFCAS and the test cables were proposed. To improve the users' experience, conductive textile was selected as the main material of the signal layer, the shielding layer, and the ground layer. All insulation layers were made of laminating film. To conduct reliable experiments, the sizes of signal layer, shielding layer, and ground layer were set to  $4.0 \text{ cm} \times 4.0 \text{ cm}$ ,  $5.0 \text{ cm} \times 5.0 \text{ cm}$ , and  $6.0 \text{ cm} \times 6.0 \text{ cm}$ , respectively. After the final lamination, the thickness of the NFCAS's plate was limited to only 0.40 mm. The NFCAS's model was also discussed.

From Figure 3, the NFCAS's capacitance had an inverse ratio to the angle, which corresponds to the Equation (1). However, the NFCAS's measurement capacitance was larger than its computed results based on the Equation (1), which were more obvious for the smaller angle. At the same time, when the angle was larger than  $80^\circ$ , the change of the NFCAS's capacitance was insignificant. In the FEA experiment, the 2D model of the NFCAS was used and its results followed computational results of the Equation (1) via Matlab. However, in the 2D FEA model, part fringe effect was ignored and its results had a small deviation from the three dimensional (3D) FEA model, which was closer to the real model of the NFCAS. The inconsistency results might be also caused by other factors, including the long test cables, the non-ideal property of the drive cable circuit, the fringe effect, and the NFCAS's motion caused by involuntary muscle movements.

From Figure 4, the forearm's states including muscle relaxation, muscle contraction, and rotation, affected both the NFCAS's results and the MPU6050s' results significantly. Thus, the forearm's states

would cause extra errors for the angle measurement with the NFCAS. Angle standard deviations of the MPU6050s were small, while those of the NFCAS were larger, especially those for larger angles.

During push-ups and push-pulls exercises, involuntary muscle movements would lead to the NFCAS's motion, which may cause extra measurement errors. The parasitic capacitance of the long cables is tens of picofarads per meter, which may cause extra parallel capacitance for the NFCAS. In the prototype detection system of the NFCAS, drive cable technology realized by the operational amplifier with its closed loop gain of 1 was used to eliminate the parasitic capacitance of the long cables and the fringe effect of the NFCAS's plates. However, an ideal closed loop gain of 1 with the operational amplifier is still difficult to achieve. Thus, complete elimination of parasitic capacitance and fringe effect is extremely challenging. From the experimental results in Figures 4, 8 and 10, the NFCAS is suitable for the detection of small angle movements ( $30^{\circ}$ – $90^{\circ}$ ) of human limbs, while for large angles, its sensitivity is decreased.

The NFCAS is soft, thin, light weight, and easily-made. Compared to Kinect sensor [1,2], the NFCAS is mounted on the surface of garment and can be easily worn or removed by using hook-and-loop and standard snap fasteners. Thus, the NFCAS is more suitable for detecting human body motion during outdoor physical exercises. Compared with IMU sensor [4–6] and M-IMU sensor [7], the NFCAS needs less post-processing. In particular, the special structures of plates of the NFCAS and signal cables give the NFCAS strong anti-interference capabilities. The NFCAS is made of soft materials which introduce less dyskinesia. Compared with strain resistive sensors [3,5,9,10], the NFCAS doesn't need any steady fabric to fix the sensor. Thus, the NFCAS works with less discomfort and less extra dyskinesia. Compared with strain capacitive sensors [8], the NFCAS doesn't need any direct contact with skin of joint which is more practical and more comfortable in real-world scenarios.

In this study, we presented the NFCAS, which is useful for detecting human limb motion in physical exercises. In future studies, we will attempt to make the NFCAS softer by changing the materials of insulation layers, and able to detect more complex human motions with multiple NFCASs.

**Author Contributions:** Conceptualization, J.-F.W. and Y.W.; Data curation, J.-F.W., Y.W., C.Q., R.Z., Z.-P.C., X.-G.Z., S.-S.H., F.W., Q.W. and J.-Q.L.; Investigation, J.-F.W. and C.Q.; Supervision, J.-F.W. and J.-Q.L.; Validation, J.-F.W., C.Q. and Y.W.; Writing—original draft, J.-F.W. and Y.W.

**Funding:** This research was supported in part by the Fundamental Research Funds for the Central Universities, and in part by the Program for Postgraduates Research Innovation in the University of Jiangsu Province under Grant SJLX16\_0074, SJCX17\_0045 and KYCX17\_0067. This research was also supported by the Foundation of State Key Laboratory of Robotics (No. 2017-O14) and the International S&T Cooperation Program of China (052014ZR0477).

**Conflicts of Interest:** The authors declare no conflict of interest.

## Abbreviations

The following abbreviations are used in this manuscript:

2D	Two dimensional
3D	Three dimensional
EEL	Exciting electrode layer
EEP	Exciting electrode plate
ESL	Exciting shield layer
FEA	Finite element analysis
GL	Ground layer
IMU	Inertial measurement units
M-IMU	Magneto and inertial measurement unit
NFCAS	Novel flexible capacitive angle sensor
SEL	Sensing electrode layer
SEP	Sensing electrode plate
SSL	Sensing shield layer

## References

1. Chuang, C.H.; Chen, Y.N.; Deng, M.S.; Fan, K.C. Gesture Recognition Based on Kinect. In Proceedings of the 2016 IEEE International Conference on Cyber Technology in Automation, Control, and Intelligent Systems, Chengdu, China, 19–22 June 2016. [CrossRef]
2. Kurillo, G.; Chen, A.; Bajcsy, R.; Han, J.J. Evaluation of upper extremity reachable workspace using Kinect camera. *Technol. Health Care* **2013**, *21*, 641–656. [CrossRef] [PubMed]
3. Bianchi, M.; Haschke, R.; Büscher, G.; Ciotti, S.; Carbonaro, N.; Tognetti, A. A multi-modal sensing glove for human manual-interaction studies. *Electronics* **2016**, *5*, 42. [CrossRef]
4. Seel, T.; Raisch, J.; Schauer, T. IMU-Based Joint Angle Measurement for Gait Analysis. *Sensors* **2014**, *4*, 6891–6909. [CrossRef] [PubMed]
5. Coates, J.; Chipperfield, A.; Clough, G. Wearable multimodal skin sensing for the diabetic foot. *Electronics* **2016**, *5*, 45. [CrossRef]
6. Imtiaz, M.H.; Ramos-Garcia, R.I.; Senyurek, V.Y.; Tiffany, S.; Sazonov, E. Development of a Multisensory Wearable System for Monitoring Cigarette Smoking Behavior in Free-Living Conditions. *Electronics* **2017**, *6*, 104. [CrossRef] [PubMed]
7. Ricci, L.; Formica, D.; Sparaci, L.; Lasorsa, F.R.; Taffoni, F.; Tamilia, E.; Guglielmelli, E. A New Calibration Methodology for Thorax and Upper Limbs Motion Capture in Children Using Magneto and Inertial Sensors. *Sensors* **2014**, *1*, 1057–1072. [CrossRef] [PubMed]
8. Atalay, A.; Sanchez, V.; Atalay, O.; Vogt, D.M.; Haufe, F.; Wood, R.J.; Walsh, C.J. Batch Fabrication of Customizable Silicone-Textile Composite Capacitive Strain Sensors for Human Motion Tracking. *Adv. Mater. Technol.* **2017**, *9*. [CrossRef]
9. Shyr, T.W.; Shie, J.W.; Jiang, C.H.; Li, J.J. A Textile-Based Wearable Sensing Device Designed for Monitoring the Flexion Angle of Elbow and Knee Movements. *Sensors* **2014**, *3*, 4050–4059. [CrossRef] [PubMed]
10. Nakamoto, H.; Ootaka, H.; Tada, M.; Hirata, I.; Kobayashi, F.; Kojima, F. Stretchable Strain Sensor with Anisotropy and Application for Joint Angle Measurement. *IEEE Sens. J.* **2016**, *10*, 3572–3579. [CrossRef]
11. Kim, M.; Moon, W.; Yoon, E.; Lee, K.R. A new capacitive displacement sensor with high accuracy and long-range. *Sens. Actuators A Phys.* **2006**, *130*, 135–141. [CrossRef]
12. Zhou, M.X.; Huang, Q.A.; Qin, M.; Zhou, W. A novel capacitive pressure sensor based on sandwich structures. *J. Microelectromech. Syst.* **2005**, *14*, 1272–1282. [CrossRef]
13. Chiang, C.T.; Huang, Y.C. A Semi cylindrical Capacitive Sensor with Interface Circuit Used for Flow Rate Measurement. *IEEE Sens. J.* **2006**, *6*, 1564–1570. [CrossRef]
14. Yang, Q.; Andrew, J.Y.; Simonton, J.; Yang, G.; Dohrmann, Y.; Kang, Z.; Li, Y.; Mo, J.; Zhang, F.Y. An inkjet-printed capacitive sensor for water level or quality monitoring: Investigated theoretically and experimentally. *J. Mater. Chem. A* **2017**, *5*, 17841–17847. [CrossRef]
15. Kanaparthi, S. Pencil-drawn Paper-based Non-invasive and Wearable Capacitive Respiration Sensor. *Electroanalysis* **2017**. [CrossRef]
16. Patla, B.R. Small Angle Approximation for Non-parallel Plate Capacitors with Applications in Experimental Gravitation. *arXiv* **2012**, arXiv:1208.2984.
17. AD7746 Datasheet. Available online: <http://www.alldatasheet.com/datasheet-pdf/pdf/539122/AD/AD7746.html> (accessed on 1 August 2018).
18. Qin, D.P. A simplified calculation of the electric field and the capacitance for a non-parallel plate capacitor. *Coll. Phys.* **1995**, *1*, 13–14. (In Chinese) [CrossRef]
19. Zhao, J.Y.; Fan, Y.M.; Zhang, G.X. The intelligent Capacitance-Micrometer. *Electron. Meas. Technol.* **2006**, *4*, 11–12. (In Chinese) [CrossRef]
20. Tokarska, M.; Gniotek, K. Anisotropy of the electrical properties of flat textiles. *J. Text. Inst.* **2015**, *106*, 9–18. [CrossRef]

